PUBLICATIONS OF THE ASTRONOMICAL SOCIETY OF THE PACIFIC
101: 816–831, September 1989

NEWBORN STARS AND STELLAR WINDS IN BARNARD 228

MARK H. HEYER*‡ AND J. A. GRAHAM †‡

Department of Terrestrial Magnetism, Carnegie Institution of Washington, 5241 Broad Branch Road NW, Washington, DC 20015

Received 1989 March 17, revised 1989 June 5

ABSTRACT

Imaging and spectroscopic observations of pre-main-sequence stars in the B228 molecular cloud have identified three sites of extended, shock-excited nebulosity. A highly collimated, blueshifted jet is associated with the T Tauri star Sz68 (CoD −33°10685). A candidate Herbig-Haro object is found near Sz68 and the T Tauri star Sz69. A third region of shock-excited nebulosity is identified near the embedded newborn star IRAS 15398-3359. Infrared excesses observed toward these stellar sources may imply a relationship between outflow activity and the presence of a circumstellar disk. Only one of the two outflow sources with well-defined orientations is aligned with the large-scale, magnetic-field geometry of the cloud in contrast to the global alignment of outflows in the Taurus cloud complex. Data for three previously unidentified emission-line stars are presented. In particular, we identify a faint 18th magnitude dMe star located 48″ west of Sz68.

Key words: nebulae: stellar winds–star formation

1. Introduction

Highly collimated mass outflows are a common feature to the pre-main-sequence evolution of all stars. Signatures of youthful stellar wind activity, identified at the earliest stages of star formation, include high-velocity CO emission from a shell of accelerated ambient material (Snell, Loren, and Plambeck 1980) and Herbig-Haro object nebulosity produced by shock interactions. At later stages of pre-main-sequence evolution, when the stars are optically visible, P Cygni line profiles of chromospheric emission attest to the presence of outflowing material very close to the star (Kuhi 1964). Given the likely role stellar winds play in the termination of the accretion process (Shu, Adams, and Lizano 1987), the regulation of stellar angular momentum (Weber and Davis 1967), and the energetics of the parent molecular cloud (Norman and Silk 1980), a more complete description of the outflow phenomena is necessary in order to gain a more comprehensive understanding of the star-formation process.

A full accounting of the mass outflow activity within an individual star-forming region may provide insight into the processes and mechanisms responsible for stellar winds at various stages of pre-main-sequence evolution and the structural impact of these winds on the parent cloud. From a survey of optically identified mass outflows within the Taurus and Orion star-forming regions, Strom *et al.* (1986) find that these directed outflows are generally aligned with the large-scale, magnetic-field orientation of the cloud and proposed a prominent role of the interstellar magnetic field in the collimation and orientation of focused stellar winds. More recently, Strom *et al.* (1988*b*) find a correspondence of stellar wind signatures with infrared excesses from the spectral energy distribution of the pre-main-sequence stars in the Taurus clouds. From these observations Edwards and Strom (1987) suggest a correspondence between energetic pre-main-sequence stellar winds and an accreting, circumstellar disk.

The B228 dark cloud (Barnard 1927) is a component clump within a larger molecular cloud complex (Murphy, Cohen, and May 1986). While the mass of the cloud complex is large (10^4 $M_\odot$; Murphy *et al.* 1986) there is no history of massive star formation, although there could be a remote connection with the more distant Scorpio Centaurus association. Like the Taurus cloud regions, B228 has long been known to contain isolated T Tauri and emission-line stars (Henize 1954; Schwartz 1977). Evidence for a magnetically dominated gas dynamics similar to that found in Taurus (Heyer *et al.* 1987) is provided by recent polarization measurements of background stars which reveal an ordered magnetic-field geometry threading the narrow cloud filaments (Strom, Strom, and Edwards 1988*a*). Given these similarities, the Lupus cloud complex provides an appropriate region to compare the associated mass outflow activity and the spectral proper-

*Visiting Astronomer, Las Campanas Observatory.

†Adjunct Staff Member, Mount Wilson and Las Campanas Observatories.

‡Visiting Astronomer, Cerro Tololo Inter-American Observatory, operated by AURA, Inc. under contract to the National Science Foundation.

ties of newborn stars to those found in the Taurus clouds.

In this paper we report the detection and physical characteristics of extended signatures to stellar wind activity in the B228 cloud from optical imaging and spectroscopic observations of pre-main-sequence objects. Most of these sources are emission-line stars which exhibit several well-known characteristics of stellar youth and were detected from a previous objective-prism survey of the region (Schwartz 1977). We have supplemented this list with objects selected from the *IRAS Point Source Catalog* (1985) which are coincident with regions of high visual obscuration. Since our source list is biased toward known, optically identified stars, our study does not constitute a complete sampling of outflow activity in this cloud. In addition, we report results of stellar spectroscopy and infrared photometry of the stellar sources in order to characterize those objects found to be associated with mass outflow activity by chromospheric and circumstellar features.

2. Observations

The fields we have examined are listed in Table 1 with 1950 epoch coordinates and red magnitudes estimated by Schwartz (1977). Our initial aim was to compare images obtained with a broad-band (1000 Å, FWHM) red filter (R) and with a narrow-band (30 Å, FWHM) filter centered on Hα. The Swope 1-m telescope of Las Campanas Observatory was used with an RCA 308 × 512 CCD detector. Each frame covered a field 4.6 by 7.4 arc minutes. Total exposures were typically 240 seconds for the R filter and 3600 seconds for the Hα filter. Shorter exposures were observed and coadded to minimize saturation of the detector on bright stars. Those fields which showed evidence for extended emission were also imaged with a [S II] filter centered on wavelength 6724 Å (30 Å, FWHM) to provide an additional measure of the distribution of shock-excited nebulosity. Additional images in [S II] and Hα were obtained in June 1988 with the Swope 1-m telescope and a TI 512 × 512 CCD detector. These later frames were resampled to provide images at the RCA CCD resolution of 0.85 arc sec pixel^{-1}. Due to the large bandwidth, an image obtained with the R filter may contain a large signal from a continuum component in addition to emission from discrete nebular lines such as [O I], [N II], Hα, and [S II]. The narrow-band images, on the other hand, predominantly show the light radiated at the wavelength of the emission lines.

In addition to providing the sites of shocked gas and identifying locations where light is scattered from an obscured, embedded source, the R and Hα frames can be used to search for faint Hα emission-line stars by using the image monitor in a blink comparator mode. The greatly different filter bandpasses cause those stars whose emission is mostly in the Hα line to be distinguished from other nonemission-line stars in the field. With this technique we can detect emission-line stars more than 2 magnitudes fainter than with conventional objective-prism techniques (e.g., Schwartz 1977). The disadvantage is the small field of the CCD detectors as used at present. However, with the increasing size of the detectors and their adaption to Schmidt telescopes, this could prove a very effective technique to detect faint emission-line stars at the low end of the luminosity function.

Optical spectra have been obtained of most of the known objects in the B228 cloud which are relevant to early stellar evolution. The 4-m telescope at Cerro Tololo Inter-American Observatory (CTIO), the Ritchey-Chrétien spectrograph, and a GEC CCD detector were used for this work during an observing run on 1988 June 2–5. Our work was carried out at two dispersions, one using the KPGL D grating covering a wavelength range 6200 Å– 6900 Å. In this case the resolution corresponded to 1.2 Å pixel^{-1}. On 1988 June 4 a second configuration using grating 400 was used to obtain a spectral range 5700 Å– 8900 Å with a resolution of 5.7 Å pixel^{-1}. In both cases, a slit width of 150 μm (1 arc sec) was used and a

TABLE 1

Source List

Name	α(1950)	δ(1950)	m_R
Sz65	15^h 36^m 16.3^s	-34° 36′ 34″	12.4
Sz66	15 36 16.9	-34 36 35	14.9
15398-3359[a]	15 39 51.2	-33 59 36	17.8
Sz68	15 42 01.4	-34 08 08	9.9
Sz69	15 42 06.0	-34 09 06	15.0
Sz70	15 43 31.1	-34 20 55	15.3
Sz71	15 43 32.8	-34 21 19	13.4
Sz73	15 44 43.9	-35 05 23	14.5
Sz74	15 44 52.1	-35 06 41	13.0

[a] Position is from the *IRAS* Point Source Catalog and m_R is estimated from the R image presented in this study. A more refined position is presented in the text.

He-Ne-Ar comparison lamp provided a reference for wavelength calibration. The low-resolution spectra are suitable for line identification and to study the energy distribution. The intermediate resolution spectra can be used to extract accurate radial velocities (Graham and Heyer 1988). Intensities were calibrated by observing standard stars LTT7379 and Feige 110 whose intensities over the observed wavelengths have been established by Stone and Baldwin (1983).

When observing at intermediate resolution, we gave priority to obtaining good radial velocity and line intensity measurements for the gaseous emission regions using the images of [S II] and Hα emission as a likely guide to interaction sites between a stellar wind and the ambient cloud material. The low-resolution spectra were useful to identify the Ca II λ8500 triplet which, when observed in emission, provides a clear signature of chromospheric activity in the star (Herbig and Soderblom 1980).

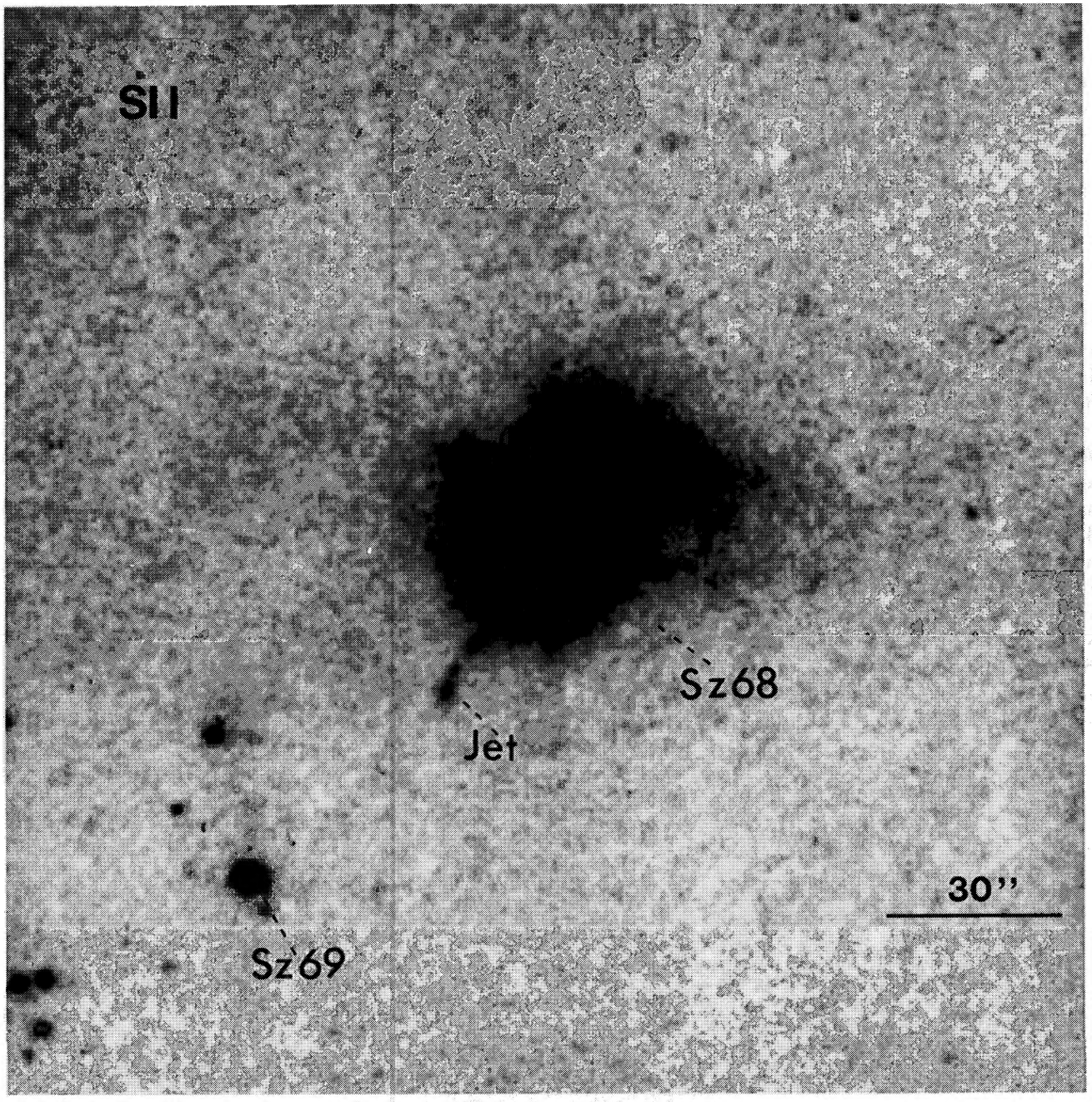

FIG. 1–CCD narrow-band (30 Å bandpass) images of the Sz68/69 region in (a) the forbidden line emission of [S II] and (b) Hα emission. A highly collimated jet of shock-excited emission extends from Sz68 at a position angle of 135°. A secondary site of shocked nebulosity is identified in the Hα image as Object 1.

We also provide infrared photometry for several newborn stars in B228. This was obtained in June 1988 with the CTIO 1.5-m telescope using an InSb detector (J, H, K, L photometry) and a bolometer for 10-μm observations. A 9″ aperture was used for the J, H, K, and L measurements, and a 13″ aperture was used for the 10-μm observations. Standard stars of the CIT-CTIO system (Elias *et al.* 1982) were measured through the same apertures for calibration to the standard CTIO system.

3. Results

3.1 *Shock Excited Regions*

3.1.1 *Sz68/69*

Sz68 and Sz69 were identified by Schwartz (1977) as emission-line stars from an Hα objective-prism survey of the B228 molecular cloud although both were previously noted as pre-main-sequence objects from earlier surveys of T Tauri stars (Henize 1954; Thé 1962). Deep images of [S II] (4800-s exposure) and Hα (3600-s exposure) emis-

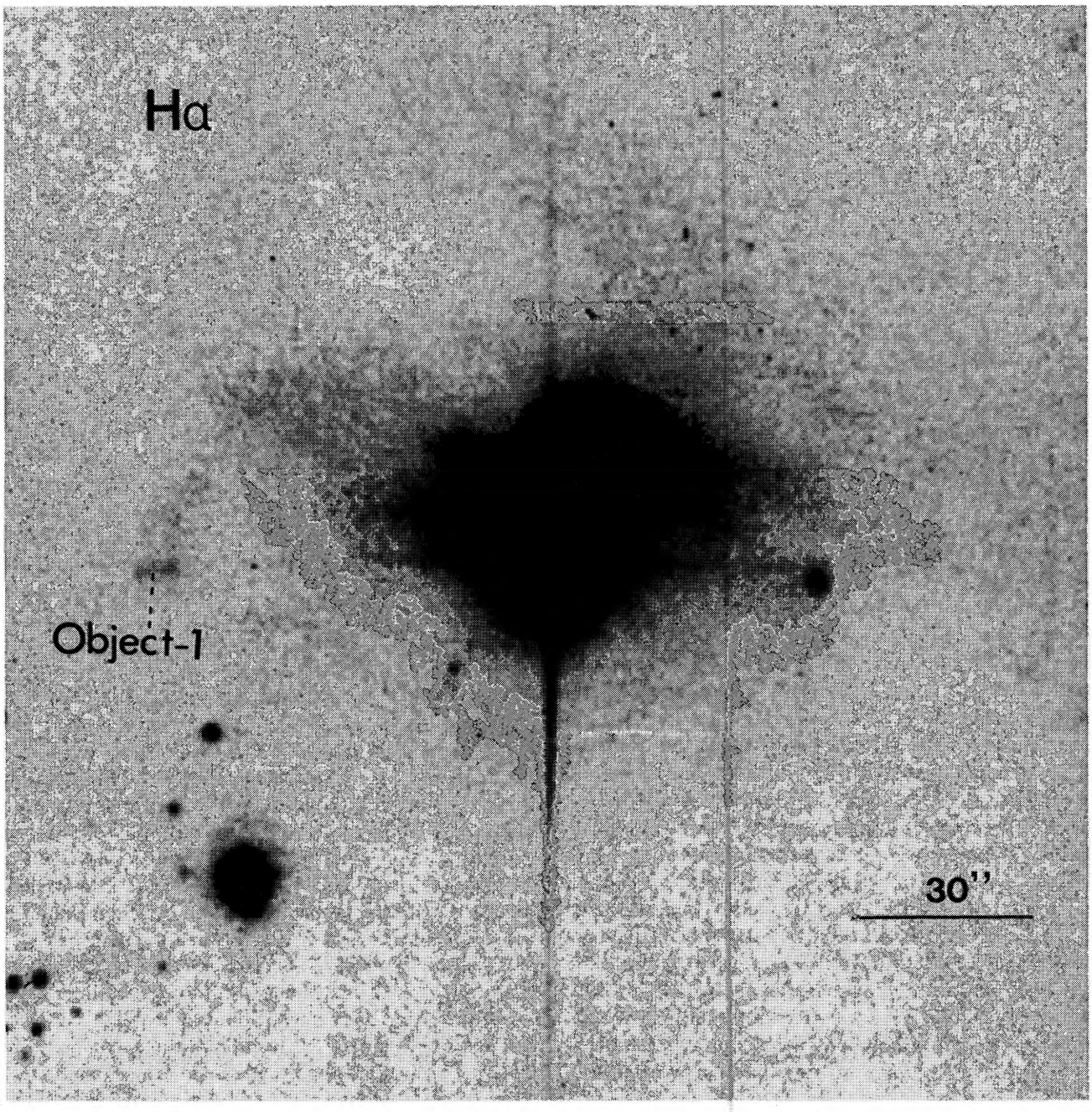

FIG. 1–CCD narrow-band (30 Å bandpass) images of the Sz68/69 region in (a) the forbidden line emission of [S II] and (b) Hα emission. A highly collimated jet of shock-excited emission extends from Sz68 at a position angle of 135°. A secondary site of shocked nebulosity is identified in the Hα image as Object 1.

sion from this field are presented in Figure 1. The circumstellar environment of Sz68 is dominated by reflection nebulosity to the northeast and northwest of the star. Removed from this reflection nebulosity but continguous to Sz68 is a highly collimated jet of forbidden [S II] emission extending 34″ at a position angle of 135°. The jet is composed of three emission peaks 21″, 28″, and 34″ from the star. We label the two strongest peaks located 21″ and 34″ from Sz68 as knot A and knot B, respectively. These emission peaks are not colinear. The position angle of the jet increases 5° counterclockwise from knot A to knot B. The axial ratio (length to diameter) of the jet, determined from the [S II] image, is 13. Hα emission from this feature is much weaker and more diffuse relative to the extended [S II] emission but reveals the clumpy composition of the jet. The inhomogeneous appearance of the Sz68 jet is characteristic of many extended but well-collimated regions of shock excited nebulosity associated with pre-main-sequence stars and may reflect internal shocks within the stellar wind (e.g., HH34; Reipurth *et al.* 1986; Bührke, Mundt, and Ray 1988). From our observations there is no evidence for a counter jet on the opposite side of Sz68. However, a direct photograph taken by one of us at Las Campanas Observatory on 1988 June 11 reveals a looplike feature at a position angle of −45° within the reflection nebula (Graham 1988). This feature may represent scattered starlight by dust grains within the inner edges of a cavity excavated by a stellar wind on the northwest side of Sz68.

Spectrograms at intermediate and low dispersion were obtained with a slit position angle of 135° along the jet axis and which passed through Sz68 and Sz69. We reproduce the intermediate dispersion spectrogram as Figure 2. The extracted spectra of knot A and knot B are shown in Figure 3. Each knot exhibits low-excitation forbidden line emission ([O I] [N II], [S II]) as well as Hα. These spectral features are characteristic of many HH objects and other jet sources (Schwartz 1983; Mundt, Brugel, and Bührke 1987). We note the presence of an unidentified emission line at λ6520 in these spectra which we suspect to be an artifact of the sky subtraction process. From the radial velocities of the emission lines we derive mean heliocentric velocities of -47 ± 2 and -21 ± 8 km s^{-1} for knot A and knot B, respectively, where the quoted uncertainties are 1-σ deviations. The heliocentric velocity of the molecular cloud is $\approx +4$ km s^{-1} (Murphy *et al.* 1986). Since Sz68 illuminates the surrounding reflection nebulosity, we can estimate its heliocentric velocity from the measured wavelength of scattered Hα emission. From a spectrum of the reflection nebulosity, we determine a heliocentric velocity of +7.7 km s^{-1} for Sz68. Thus, the jet is a kinematically distinct feature with respect to the ambient, quiescent gas of the parent cloud and the exciting star.

The excitation conditions of the jet are estimated from

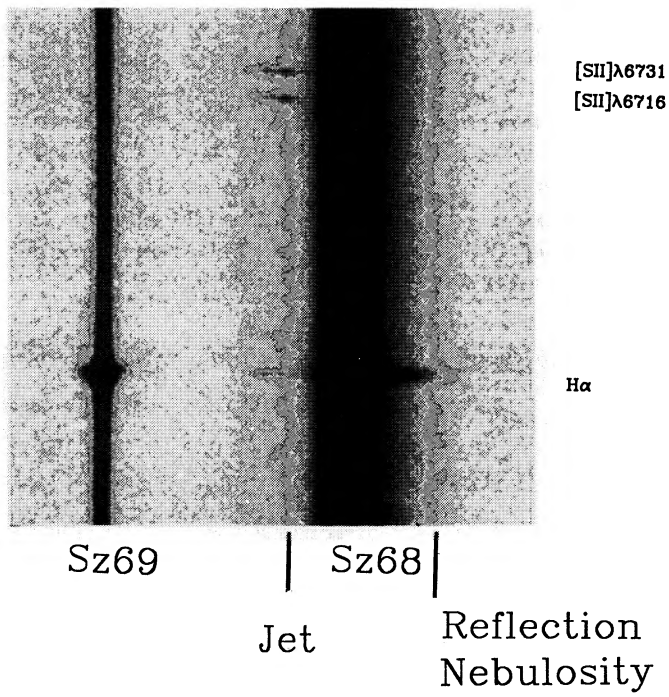

FIG. 2–A spectrogram along the axis of the Sz68 jet which also passes through Sz69, Sz68, and reflection nebulosity.

the observed ratios of the forbidden line emission. The ratio [S II] λ6716/[S II] λ6731 provides a measure of the postshock electron density. This ratio exhibits little variation along the jet (0.92–1.1) and indicates electron densities of 400–1600 cm^{-3} (Osterbrock 1989). The shock velocity is estimated from the intensities of the forbidden line emission relative to Hα emission and a comparison with shock models. However, the planar and bow shock models for HH objects presented by Hartigan, Raymond, and Hartmann (1987) do not satisfactorily account for the observed line ratios found for the Sz68 jet—in particular, the large values of [O I] and [S II] emission relative to the measured Hα intensity. Similar excitation conditions are found in the well-studied outflow associated with HH46 (Graham and Elias 1983; Schwartz 1983) in which low shock velocities with insufficient energy to dissociate molecular hydrogen are inferred. For the Sz68 jet we estimate a range of shock velocities appropriate for the observed [S II] to Hα ratio to be 20–40 km s^{-1}. A summary of the relative line intensities and velocities of the jet is listed in Table 2.

An additional, very faint region of extended nebulosity is identified in the Hα image of the Sz68/69 field. It is located 72″ from Sz68 at a position angle of 90°. We label this feature as Object 1. This nebulosity is composed of two knots separated by 3″ and which are oriented east-west. No [S II] counterpart to this nebulosity is detected in these images. An intermediate dispersion spectrum of Object 1 is presented in Figure 4. Only Hα, [N II] λ6583, and [S II] λ6716 are clearly seen in emission. [S II] λ6731

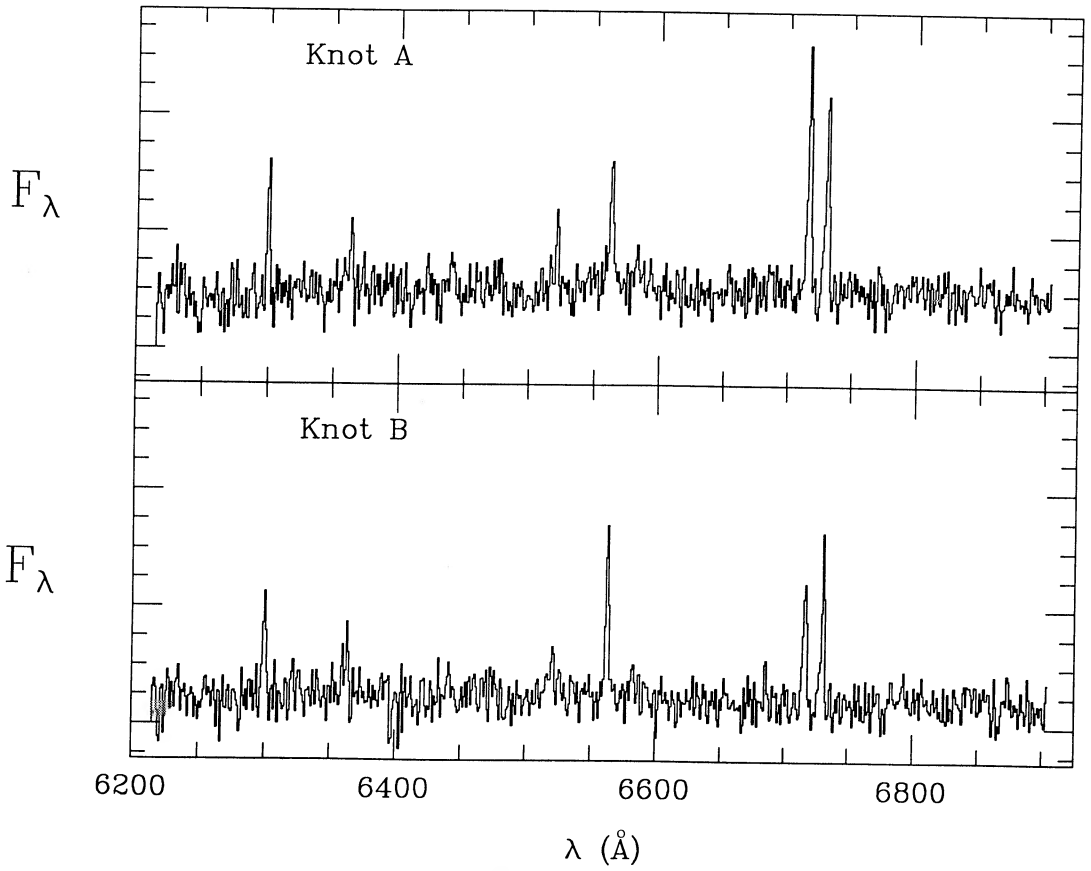

FIG. 3–Intermediate dispersion spectra from the positions of peak shock-excited nebulosity along the Sz68 jet. Both emission peaks within the jet are characterized by low-excitation conditions and blueshifted velocities.

TABLE 2

Forbidden Emission Line Ratios and Radial Velocities

	$\frac{[OI]\lambda6300}{H\alpha}$	$\frac{[SII]\lambda6716}{H\alpha}$	$\frac{[SII]\lambda6731}{[SII]\lambda6716}$	v_{rad} [a] (km s^{-1})
Knot A	0.63	1.75	0.79	-47
Knot B	0.48	0.72	1.07	-21
Object 1	...	0.22	0.40	-28
15398-3359	2.67	1.65	1.64	-46

a) heliocentric velocity

is only marginally detected. The [S II] ratio λ6731/λ6716 is estimated to be 0.4 ± 0.2. While the line intensities alone do not demand excitation under shocked conditions, we believe this interpretation likely due to the absence of any strong photoionizing radiation sources in the area and because of the significantly negative heliocentric velocities (−28 km s^{-1}) of the Hα line. The intensity of the Hα emission relative to the [S II] λ6716 would imply shock velocities of order 40 km s^{-1} (Hartigan, Raymond, and Hartmann 1987). Low-resolution spectra for these emission nebulosities were obtained but these revealed no additional features. Specifically, we saw no underlying continuum or the Ca II λ8500 triplet lines which could be attributed to an associated star. No additional lines were detected which would confirm the shock origin for the Herbig-Haro emission.

While the location and orientation of the Object 1 emission peaks may implicate Sz68 as the central source responsible for its excitation, such an association would imply two divergent ($\Delta\theta = 45°$) but well-collimated out-

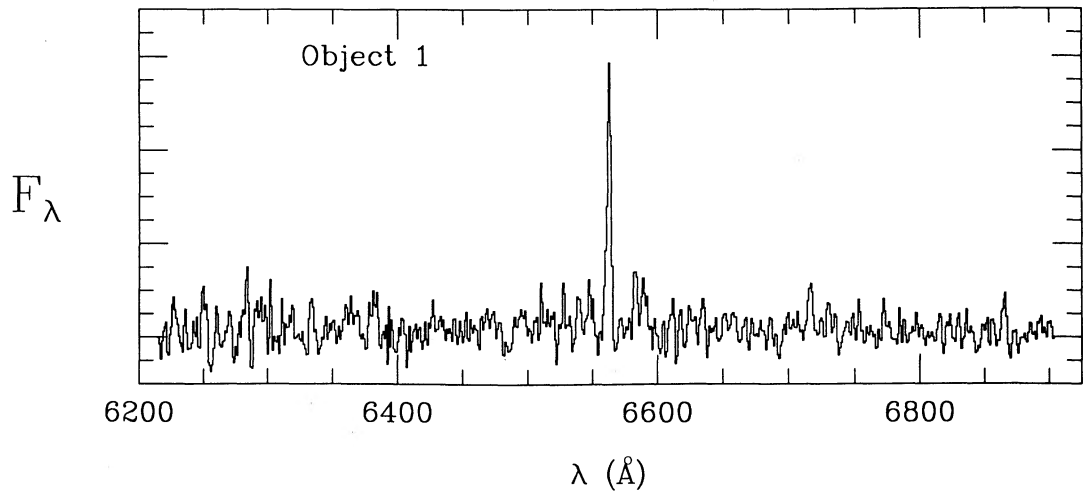

FIG. 4–Intermediate dispersion spectrum of Object 1. Based on the detection of Hα, [N II] λ6583, [S II] λ6716, and blueshifted velocities (−30 km s^{-1}), we identify Object 1 as a candidate HH object.

flows from this pre-main-sequence star. We note that the nearby active T Tauri star Sz69 is an attractive alternate source. Before a more definitive association of Object 1 with a stellar source of wind activity can be made, more information is necessary such as a proper-motion vector or a detection of extended but fainter nebulosity linking this feature to the stellar source of wind activity.

3.1.2 *IRAS 15398-3359*

The *IRAS Point Source Catalog* (1985) identifies a very red object (15398-3359) located in a region characterized by high visual extinction in the B228 cloud. Based on its location and far-infrared spectral energy distribution, this object is likely a newborn star still deeply enshrouded by cloud material. The IRAS luminosity of this object is 0.5 $L_\odot$. From the examination of the broad-band *R* and narrow-band Hα images of this field we noticed a small region of nebulosity. We estimate the red magnitude of this nebulosity to be 17.8 magnitudes. A subsequent [S II] image indicated that the [S II] lines were likely strong. In Figure 5a, the [S II] image is shown as a contour map. Faint but extended nebulosity is detected over an angular scale of 15″. It is composed of two emission peaks. The stronger peak to the southwest is pointlike and, therefore, may mark the optical counterpart to the IRAS point source. Based on astrometry of nearby stars, the position (1950 coordinates) of the nebulosity emission centroid is

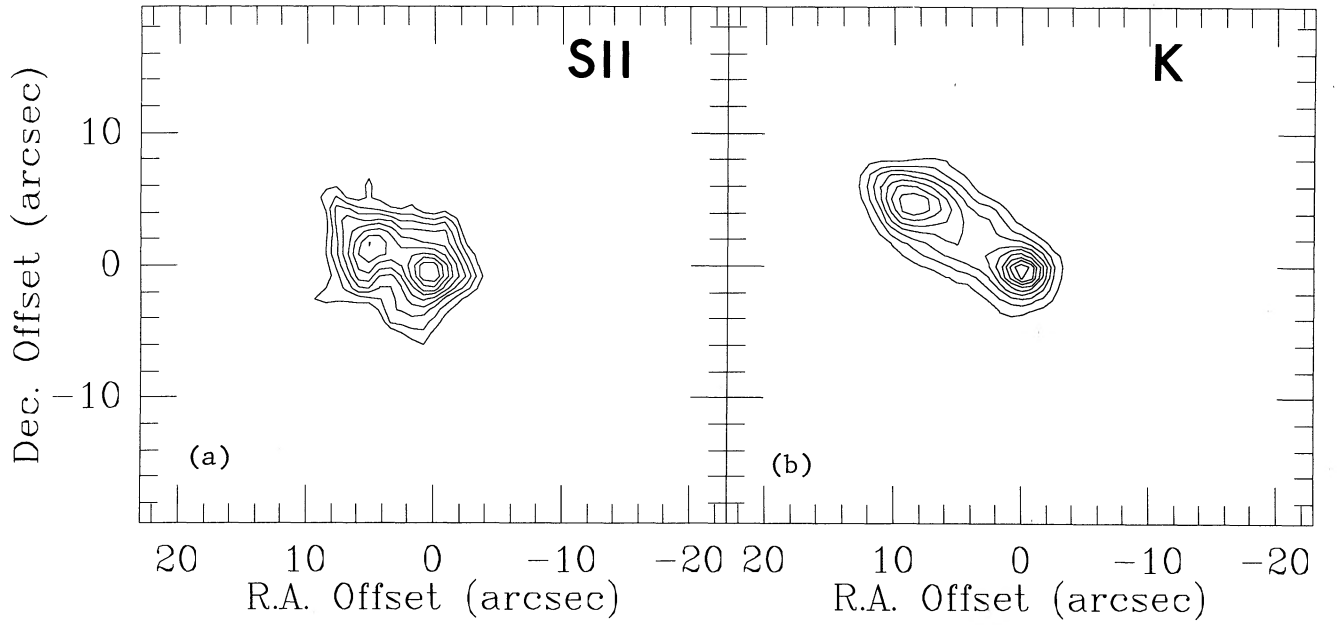

FIG. 5–Images of the 15398-3359 field. (a) Narrow-band (30 Å) [S II] emission delineating regions of shocked gas, and (b) broad-band (0.38 μ, FWHM) 2.2-μm emission. The pointlike emission peak to the southwest denotes the location of the stellar source.

(α, δ) = $15^h39^m50^s.6$, −33°59′46″.0″. Infrared images at broad-band (0.38 μm, FWHM) *K* and narrow-band (0.08 μm, FWHM) H_2 (2.12 μm) were kindly obtained by J. Elias with the CTIO 4-m telescope and the IR Imager and forwarded to us. We have estimated the contribution of the continuum to the intensity within the narrow 2.12-μm band from the broad-band *K* image and have subtracted this component from the narrow-band image. No excess emission is detected which could be attributed to shock-excited H_2 line emission. The *K*-band image, resampled to a pixel resolution of 0″.85, is shown as a contour map in Figure 5b. The pointlike nature of the southwest [S II] peak is even more pronounced in the *K* band image. We have assumed that this peak marks the position of the IRAS source. The infrared intensity distribution extends beyond the secondary peak position of the [S II] image. This extended emission may be due to light from the newborn star scattered by the surrounding dust or by dust grains within the jet. Such infrared reflection nebulosity characterizes the circumstellar environments of many newborn stars associated with mass outflow (Graham and Heyer 1989; Heyer *et al.* 1989). The extended nature of the forbidden line emission suggests that this nebulosity is excited by an energetic stellar wind from the newborn star whose location is given by the southwest point source. Our best determination of the position angle of this outflow is 65°.

To study the spectral characteristics of 15398-3359, spectrograms at both low and intermediate dispersions were obtained with the slit oriented at a position angle of 45°, our first estimate of the relative orientation of the outflow from the Hα image. These spectra are displayed in Figure 6. At intermediate dispersion strong [S II] λλ6716,6731 and [O I] λλ6300,6363 emission lines are

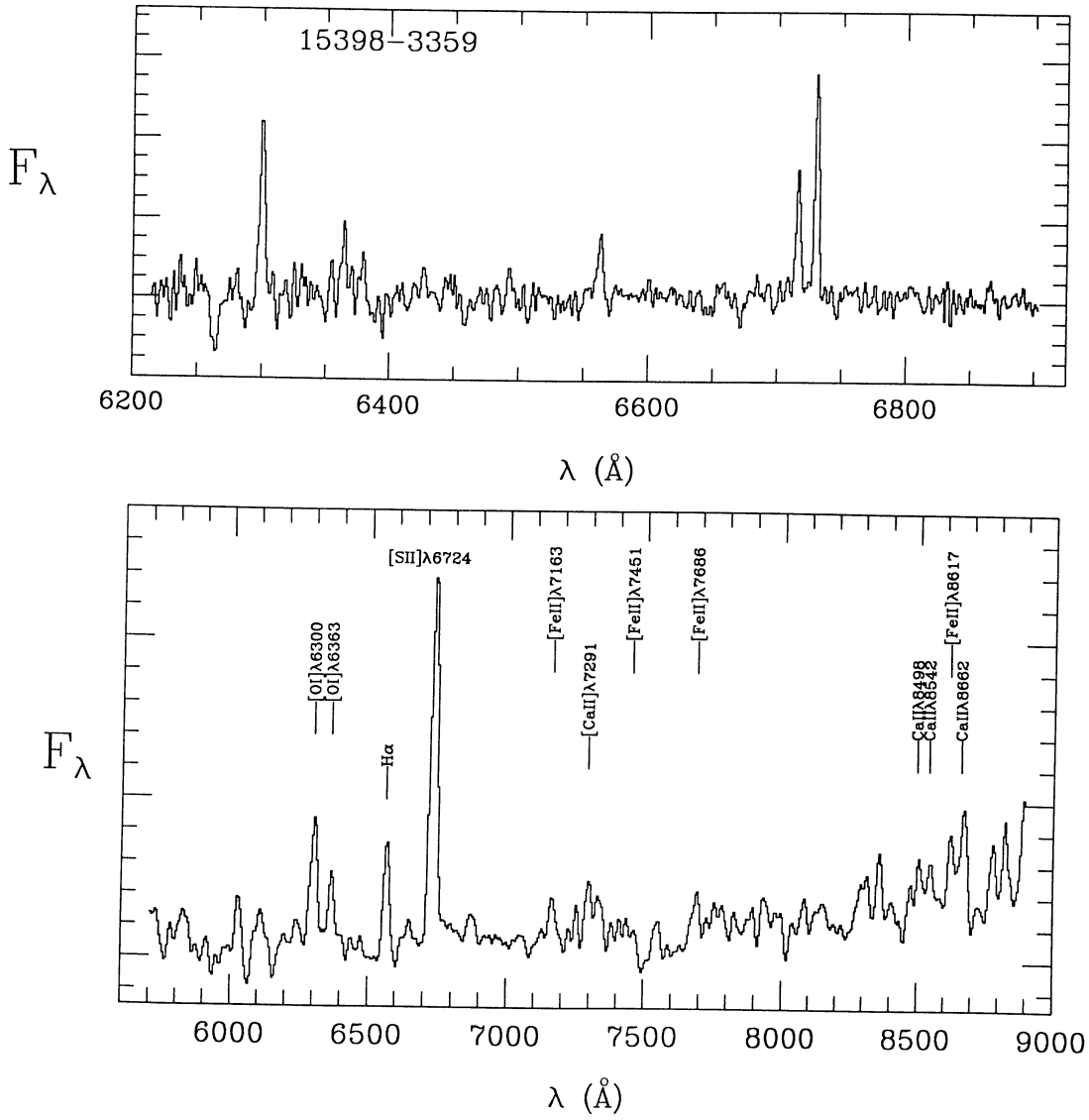

FIG. 6–Intermediate- and low-dispersion spectra of 15398-3359 showing the blueshifted, forbidden line emission [O I] λλ6300,6363 and [S II] λλ6716,6731 and weak Hα. The low-dispersion spectra identify an HH spectrum in addition to a faint stellar component.

detected in addition to Hα. In the low-dispersion spectra, we identify additional forbidden emission lines ([Fe II], [Ca II]) characteristic of HH objects. A stellar component is marked by the Ca II triplet in emission at λ8500 and a rising continuum to the red of λ8000. The heliocentric velocity of the forbidden line emission is -46 ± 6 km s^{-1}. The electron density, estimated from the observed intensities of the [S II] lines, is 5900 cm^{-3}. Low shock velocities (< 20 km s^{-1}) are inferred from the extremely weak Hα emission relative to the detected forbidden lines. Intensities and velocities of this object for the various emission lines are listed in Table 2.

3.2 *Properties of Pre-Main-Sequence Stars in the B228 Cloud*

Low-dispersion spectra of all optically identified pre-main-sequence stars in our source list are displayed in Figure 7. In Table 3 we list the approximate spectral type and the Hα equivalent width for each source. Like the Taurus clouds, B228 is a site of low-mass star formation. Two of the newborn stars (Sz69 and Sz73) are distinguished by strong Hα emission relative to the continuum level (equivalent widths > 150 Å). In addition, these sources exhibit spectroscopic evidence for outflow ([O I] λ6300 line emission) and a chromosphere (emission from the Ca II triplet λλ8498,8542,8662). The presence of such forbidden line emission in the stellar spectra may indicate shock interactions in the near vicinity of the star. We note that on the ESO/SERC sky-survey photograph, Sz73 and Sz74 show weak reflection nebulae resulting from scattered light from the necessarily close dust cloud.

The infrared spectral energy distribution of a pre-main-sequence star provides a direct probe of the surrounding dust component. Results from infrared aperture photometry uncorrected for interstellar reddening for seven of the nine surveyed objects are presented in Table 4. For those sources (Sz65 and Sz68) previously observed, there is agreement with the measured flux values (Finkenzeller and Basri 1987). IRAS detected unresolved emission toward these lines of sight; however, due to the large angular response function of the IRAS detectors, nearby pre-main-sequence sources are not resolved. In general those stellar sources associated with outflow signatures (IRAS 15398-3359, Sz68, Sz69, and Sz73) exhibit infrared excesses based on their location in the $(J-H)/(H-K)$ vs. $(J-H)$ diagram (Snell 1981). Infrared excesses, relative to the underlying photospheric continuum, are found toward many T Tauri stars and are attributed to warm grains within a circumstellar disk (Cohen and Kuhi 1979).

Using the published optical fluxes (Bouvier, Bertout, and Bouchet 1988) and the near-infrared observations presented in this study, we have calculated the intrinsic spectral energy distribution of Sz68 (Fig. 8). All fluxes have been dereddened using the interstellar extinction curve Van der Hulst No. 15 (see Johnson 1968) and $A_v = 0.96$ based on the $(V-R)$ color excess (Strom *et al.* 1989). Also plotted are the mean intrinsic fluxes tabulated by Johnson (1966) for a K2 main-sequence star and scaled such that the flux at R agrees with that of Sz68. Relative to these mean standard flux values, Sz68 exhibits a moderate infrared excess at wavelengths beyond 2.2 μm. We have calculated the parameter $\Delta K = \log(F_{2.2\ \mu m}(\mathrm{Sz68})/F_{2.2\ \mu m}(\mathrm{standard}))$ used by Strom *et al.* (1989) to quantify the infrared excess. For Sz68, $\Delta K = 0.2$ which is comparable to the mean value of ΔK derived by Strom *et al.* (1989) for classical T Tauri stars within the Taurus clouds.

A comparison of our infrared measurement of Sz69 with those of Appenzeller, Jankovics, and Krautter (1983) suggests a brightening of this object at shorter wavelengths (0.51 magnitude at H and 0.23 magnitude at K), within the past five years while the flux at L band has remained relatively constant. The Hα equivalent width of Sz69 has increased by 23% over this same time interval. Such variability is commonly observed toward T Tauri stars; however, the origin (chromospheric or circumstellar) remains uncertain.

3.3 *Sources of Mass Outflow*

The imaging and spectroscopic observations presented in the previous section identify Sz68 as the most likely stellar source responsible for the observed jet feature. In addition, Sz68 and Sz69 are candidate sources responsible for the excitation of Object 1. The third outflow identified in this study (15398-3359) is likely excited by a stellar wind from a newborn star still deeply enshrouded by associated interstellar dust and, therefore, optically faint.

TABLE 3

Spectral Types and Equivalent Widths

Name	Spectral Type	EW(Hα) (Å)
Sz65	M0	3
Sz66	M6	100
Sz68	K2	3
Sz69	M6	378
Sz70	M5	57
Sz71	M4	98
Sz73	K2	150
Sz74	M4	61

TABLE 4

Near Infrared Photometry

Name	J	H	K	L	10μm
Sz65	9.05	8.32	8.01	7.45	...
Sz66	10.22	9.43	9.07	8.44	...
15398-3359	16.59	15.94	15.33	...	...
Sz68	7.60	6.90	6.52	5.87	2.92
Sz69	10.81	9.95	9.28	8.50	...
Sz73	10.63	9.28	8.31	7.12	...
Sz74	9.09	7.98	7.28	6.40	4.56

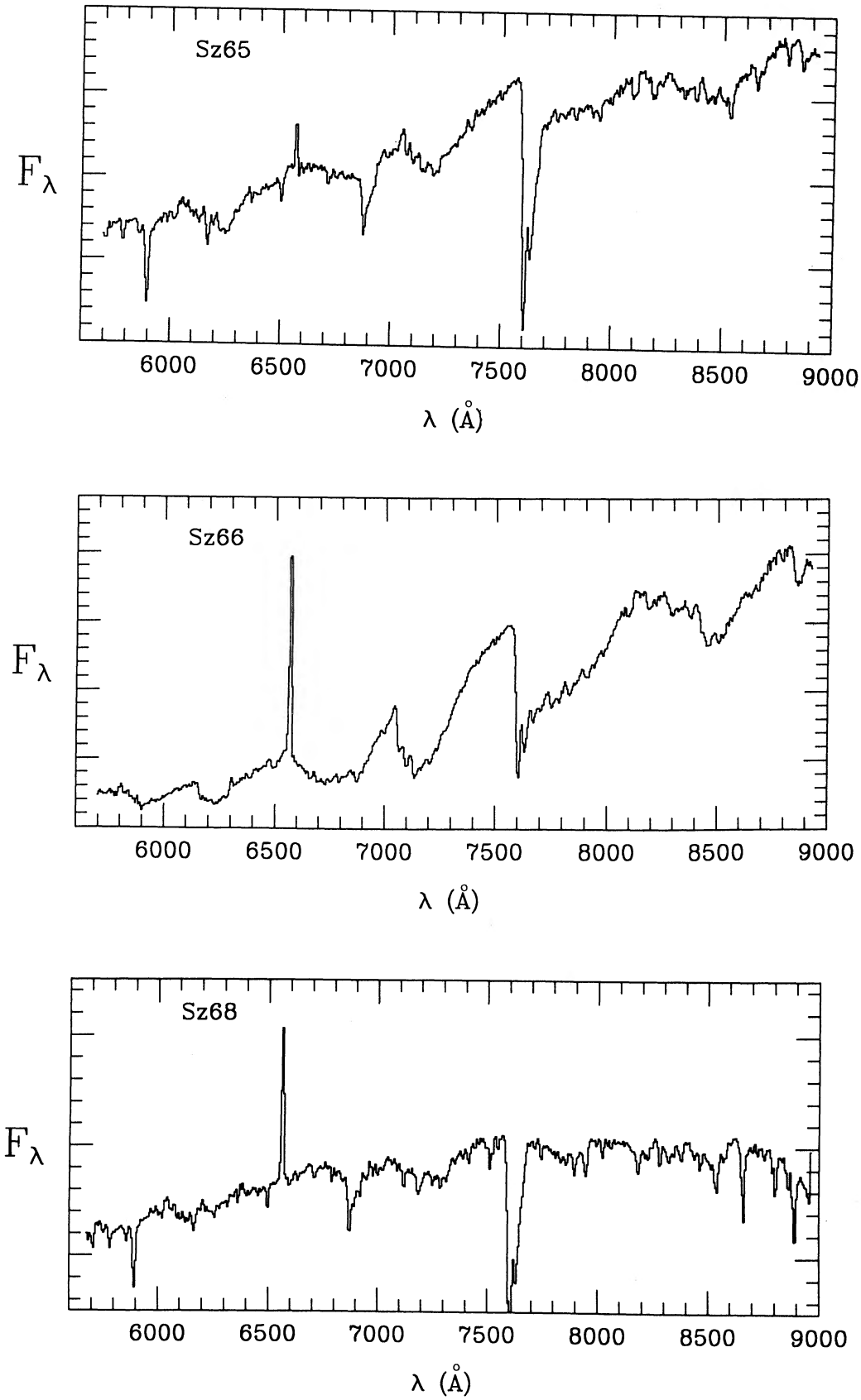

FIG. 7–Low-dispersion spectra of the optically identified T Tauri stars present in the B228 molecular cloud.

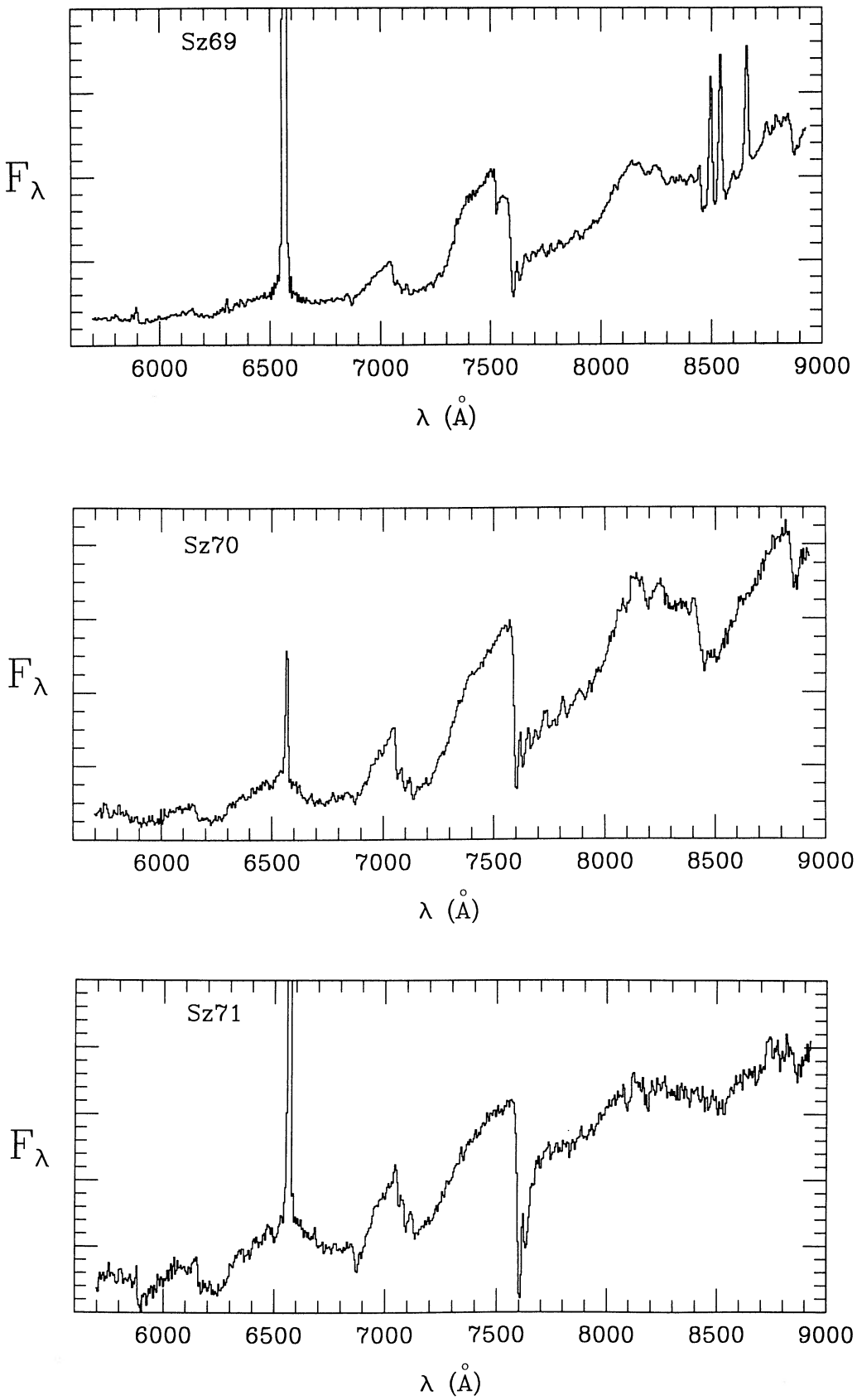

FIG. 7–Low-dispersion spectra of the optically identified T Tauri stars present in the B228 molecular cloud.

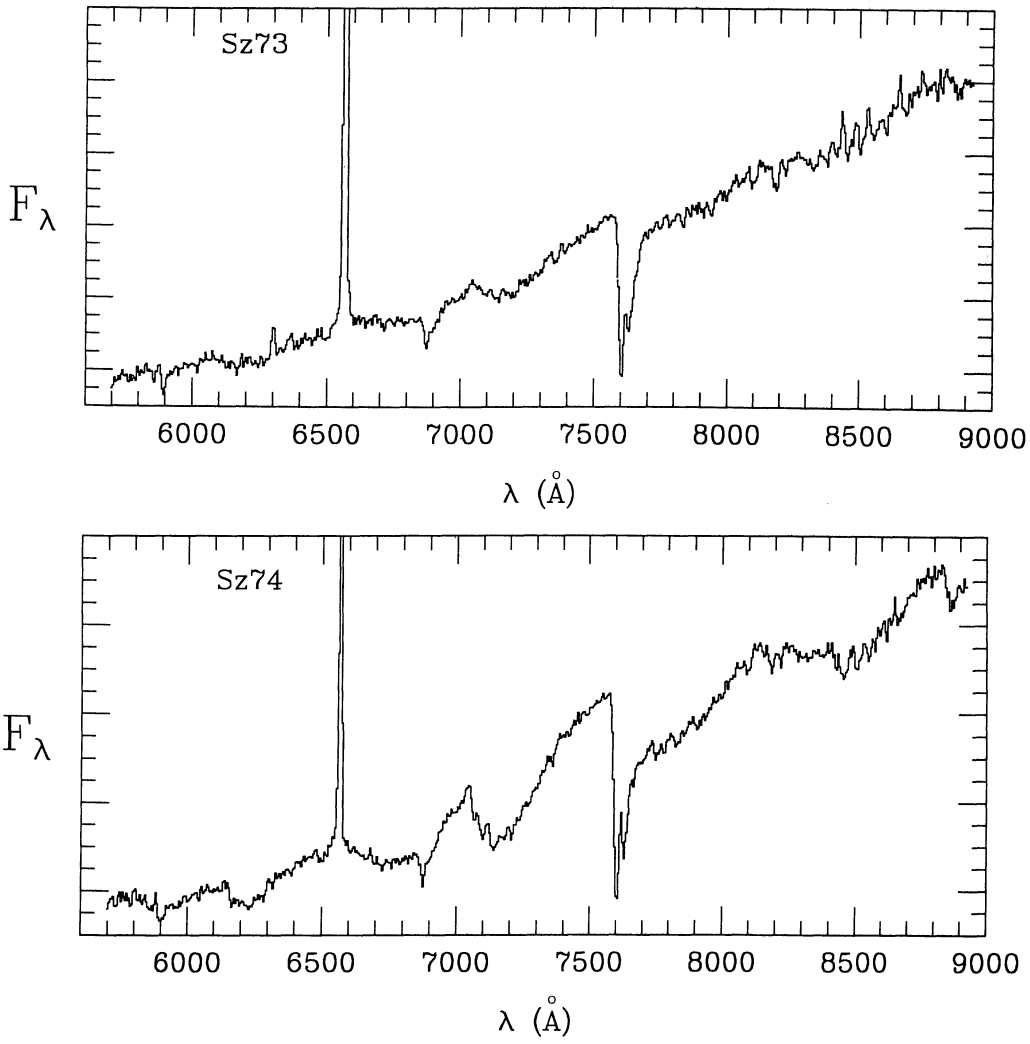

FIG. 7–Low-dispersion spectra of the optically identified T Tauri stars present in the B228 molecular cloud.

Red (6200 Å–6900 Å), intermediate dispersion spectra of Sz68 and Sz69 were observed in order to examine the kinematic relationship between these stars and the associated outflow and to determine any additional photospheric and chromospheric signatures.

The observed intermediate dispersion spectrum for Sz68 is presented in Figure 9. As previously noted by Finkenzeller and Basri (1987), the Hα profile of Sz68 exhibits a blueshifted (-51 km s^{-1}) absorption feature, a definitive signature of outflowing material (Kuhi 1964). However, we note that the self-reversal of the Hα line presented here is not as deep as seen by Finkenzeller and Basri (1987) indicating variations of the outflowing material over the last three years. With the exception of strong Hα emission, the Sz68 spectrum reveals no other emission-line features. Its photospheric spectrum is characterized by the absorption lines of Fe I and Li λ6707 (a well-known signature of stellar youth). We derive a mean heliocentric velocity of $+3 \pm 15$ km s^{-1} for Sz68 from the radial velocities calculated from these absorption lines.

The intermediate dispersion spectrum of Sz69 presented in Figure 10 shows it to be an active pre-main-sequence object. The Hα emission profile exhibits a very broad velocity component ($\Delta v_{\rm FWHM} \approx 285$ km s^{-1}) often associated with extremely active T Tauri stars (Basri 1987). The centroid velocity of the Hα line is redshifted ($+23$ km s^{-1}) which may reflect the absorption of blueward radiation by outflowing material. The intermediate dispersion spectrum of Sz69 is also characterized by the emission lines Fe II λλ6432,6456,6516 and He I λ6678 from which regions of very high temperatures (10^5 K) within the near vicinity of Sz69 are inferred. It is uncertain whether these emission lines originate within a chromosphere or boundary layer. In addition, the forbidden emission lines [O I] λλ6300,6363 are observed within the stellar spectrum. The velocities of these forbidden lines are blueshifted (-33 km^{-1}) with respect to the Fe II lines. Such negative velocity forbidden line emission is com-

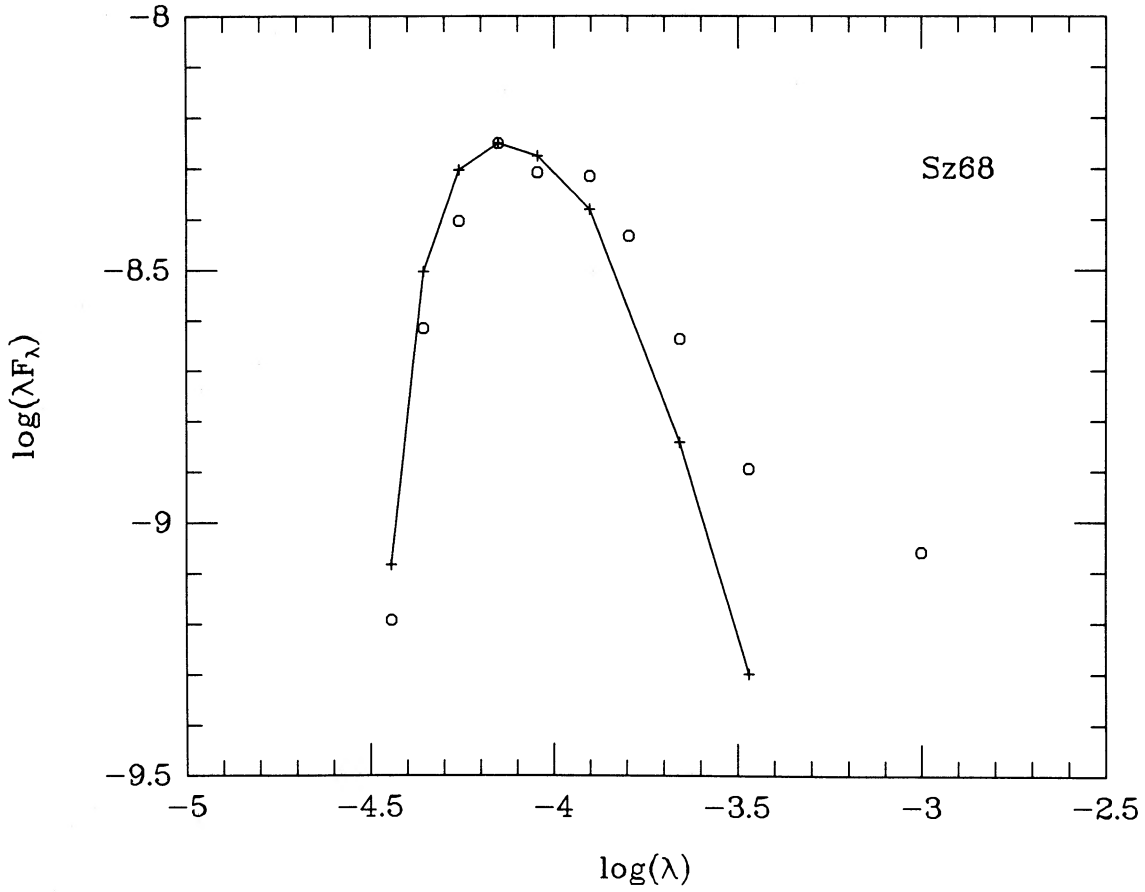

FIG. 8–The dereddened spectral energy distribution of Sz68 from 0.36 μm to 10 μm (open circles). Also shown is the spectral energy distribution of a K2 dwarf (solid line) scaled such that the flux at 0.70 μm agrees with that of Sz68.

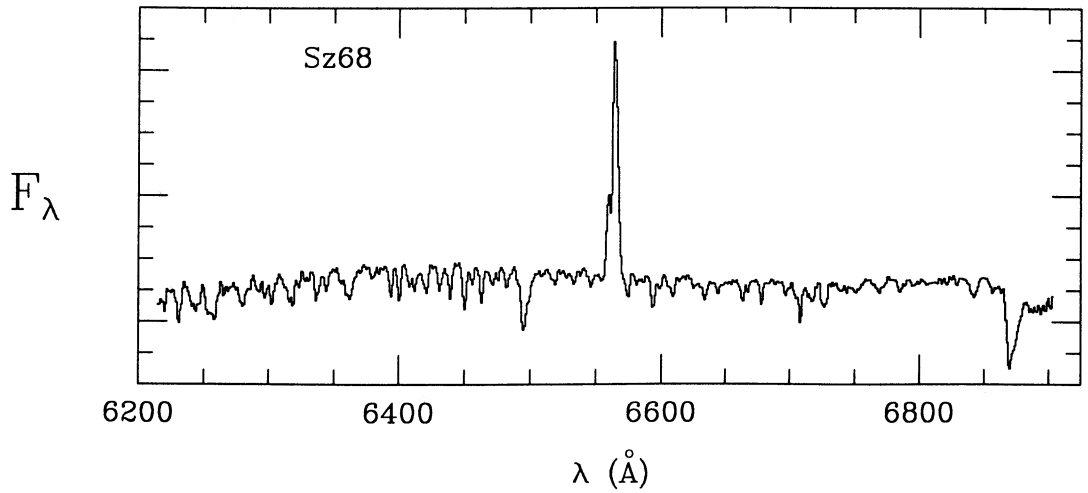

FIG. 9–Intermediate-dispersion spectrum of Sz68 showing the Fe I and Li I absorption lines and revealing the blueshifted self-reversal of the Hα line.

monly observed from T Tauri stars due to shock interactions between a stellar wind and the high-density circumstellar environment and the presence of a disk which occults the emission from the receding material (Appenzeller, Jankovics, and Ostreicher 1984; Edwards *et al.* 1987; Hartmann and Raymond 1989).

3.4 *New Emission-Line Stars*

By comparing *R* and Hα images we identified three new emission-line stars in the B228 cloud. Two of these (Hα star 1 and Hα star 2) are in the Sz68/69 field and the third (Hα star 3) is a close companion of Sz74. The low-dispersion spectra for Hα star 1 and Hα star 2 are dis-

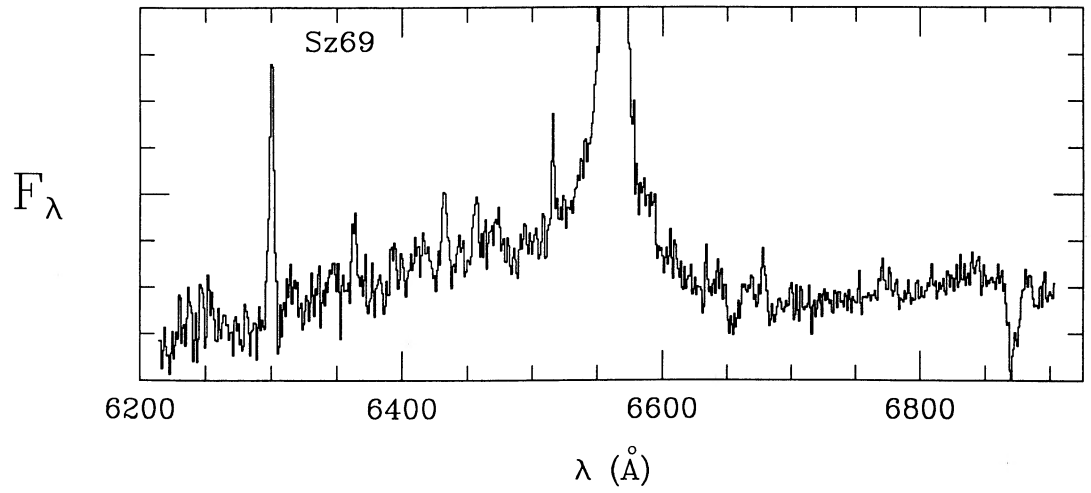

FIG. 10–Intermediate-dispersion spectrum of Sz69 showing broad Hα, emission lines of Fe II, and forbidden line emission of [O I] λ6300.

played in Figure 11. We include these stars in Table 5 with positions, red magnitudes estimated from the R image, and equivalent widths. These stars are faint $m_R \approx$ 17 magnitudes and have late M-type spectra. Many other faint emission-line stars are probably present in the B228 cloud and await detection by methods such as this.

4. Stellar Winds from Young Stars

Imaging and spectroscopic observations of newborn stars in the B228 molecular cloud have identified multiple sites of shock interaction. These observed signatures of shock excitation and high-velocity gas are likely produced by a stellar wind which often accompanies the pre-main-

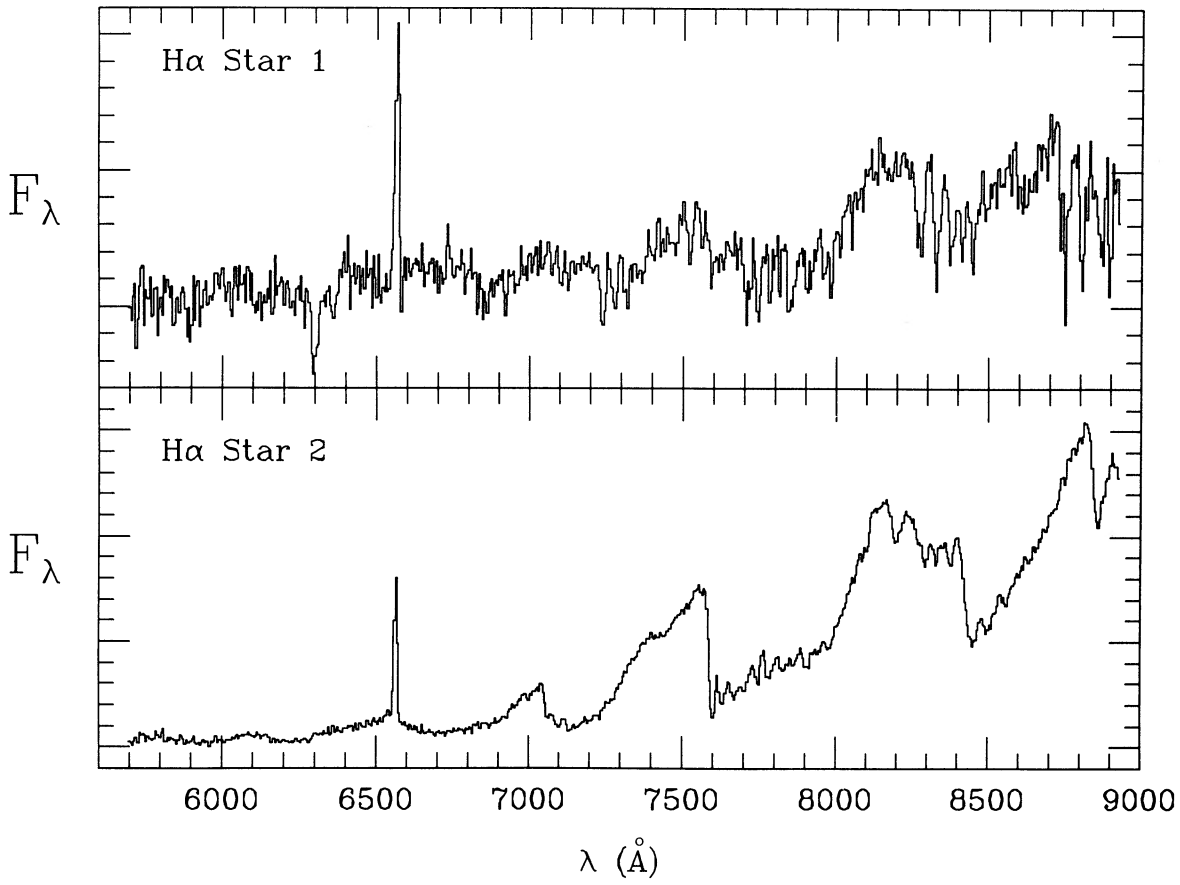

FIG. 11–Low-dispersion spectra of identified emission-line stars (a) Hα star 1 and (b) Hα star 2.

TABLE 5

Newly Identified Emission Line Stars

Hα Star	α(1950)	δ(1950)	m_R	EW(Hα)
1	15^h 41^m 57.7^s	-34° 08′ 12″	17.8	100
2	15 42 07.0	-34 12 00	16.9	132
3	15 44 53.1	-35 06 36	15.3	17

sequence evolution of a star. The stars responsible for this outflow activity include a very faint, heavily obscured candidate protostar (IRAS 15398-3359) and optically visible T Tauri stars (Sz68, Sz69, Sz73). Only a small fraction (33%) of the star surveyed in this study are associated with HH nebulosity, confirming the general absence of jets near optically identified T Tauri stars (Strom *et al.* 1988*a*). The deficiency of extended outflow signatures with T Tauri stars observed in this study cannot be attributed to the absence of ambient material since these objects were selected by their locations projected on regions of high, visual obscuration.

From our limited sample of pre-main-sequence stars within B228, we find those stars undergoing energetic mass outflow exhibit infrared excesses. From a much larger sample of young stellar objects in the Taurus clouds Strom *et al.* (1988*b*) identify a similar correlation between outflow and large infrared excesses. To account for the amount of infrared excess in the observed spectral energy distributions, Strom *et al.* (1988*a*) suggest that the disk is accreting. The energy deposited at the accretion shock-boundary layer may then be available to drive the mass outflow in addition to contributing to the observed luminosity of the star and, therefore, account for the observed correlation between wind energetics and stellar luminosity (Bally and Lada 1983).

The observed alignment of stellar jets and HH nebulosity within the Orion and Taurus star-forming regions (Strom *et al.* 1986) suggests a global cloud property, such as the interstellar magnetic field, as the primary agent responsible for the collimation and acceleration of mass outflows (Pudritz and Norman 1983; Uchida and Shibata 1985; Kwan and Tademaru 1988) or, simply, the orientation of a collimating disk structure by the magnetic braking of the cloud. Strom *et al.* (1988*a*) present a polarization map of the B228 molecular cloud. The large-scale, magnetic-field orientation of the cloud is described by a mean projected position angle of 25°. Two of the three outflows (the Sz68 jet and 15398-3359) identified in this study exhibit well-defined orientations (135° and 65°, respectively). Such nearby but misaligned outflows are not uncommon (e.g., DG Tauri and DG Tauri B; HH7-11 and HH12). The outflow associated with 15398-3359 is consistent with but not uniquely described by the magnetic collimation of the stellar wind. However, the position angles of the Sz68 stellar jet and the local magnetic-field direction are incongruent and imply that the interstellar magnetic field has not played a primary role in the collimation and orientation of this outflow.

We would like to thank Sr. Mario Hamuy and Dr. Kent Ford for their help in reduction and subsequent measurement of our spectra. J.A.G.'s work at the Department of Terrestrial Magnetism has been partly supported by NASA grant NAGW-398 to the Carnegie Institution of Washington.

REFERENCES

Appenzeller, I., Jankovics, I., and Krautter, J. 1983, *Astr. Ap. Suppl. Ser.*, **53**, 291.
Appenzeller, I., Jankovics, I., and Ostreicher, R. 1984, *Astr. Ap.*, **141**, 108.
Bally, J., and Lada, C. J. 1983, *Ap. J.*, **265**, 824.
Barnard, E. E. 1927, in *A Photographic Atlas of Selected Regions of the Milky Way*, ed. E. B. Frost and M. R. Calvert (Washington, DC: Carnegie Institution of Washington), p. 29.
Basri, G. 1987, in *Proceedings of Cool Stars, Stellar Systems, and the Sun*, ed. J. L. Linsky and R. E. Stencel (Berlin: Springer-Verlag), p. 411.
Bouvier, J., Bertout, C., and Bouchet, P. 1988, *Astr. Ap. Suppl. Ser.*, **75**, 1.
Bührke, T., Mundt, R., and Ray, T. P. 1988, *Astr. Ap.*, **200**, 99.
Cohen, M., and Kuhi, L. V. 1979, *Ap. J. Suppl.*, **41**, 743.
Edwards, S., and Strom, S. E. 1987, in *Proceedings of Cool Stars, Stellar Systems, and the Sun*, ed. J. L. Linsky and R. E. Stencel (Berlin: Springer-Verlag), p. 443.
Edwards, S., Cabrit, S., Strom, S. E., Heyer, I., Strom, K. M., and Anderson, E. 1987, *Ap. J.*, **321**, 473.
Elias, J. H., Frogel, J. A., Matthews, K., and Neugebauer, G. 1982, *A.J.*, **87**, 1029.
Finkenzeller, U., and Basri, G. 1987, *Ap. J.*, **318**, 823.
Graham, J. A. 1988, *Carnegie Institution of Washington Yearbook 87*, p. 132.
Graham, J. A., and Elias, J. H. 1983, *Ap. J.*, **272**, 615.
Graham, J. A., and Heyer, M. H. 1988, *Pub. A.S.P.*, **100**, 1529.
———. 1989, *Pub. A.S.P.*, **101**, 573.
Hartigan, P., Raymond, J., and Hartmann, L., 1987, *Ap. J.*, **316**, 323.
Hartmann, L., and Raymond, J. 1989, *Ap. J.*, **337**, 903.
Henize, K. G., 1954, *Ap. J.*, **119**, 459.
Herbig, G. H., and Soderblom, D. R. 1980, *Ap. J.*, **242**, 628.
Heyer, M. H., Ladd, E., Campbell, B., and Myers, P. C. 1989, in preparation.
Heyer, M. H., Vrba, F. J., Snell, R. L., Schloerb, F. P., Strom, S. E., Goldsmith, P. F., and Strom, K. M. 1987, *Ap. J.*, **321**, 855.
IRAS Point Source Catalog 1985, Joint IRAS Science Working Group (Washington, DC: U.S. Government Printing Office).
Johnson, H. L. 1966, *Ann. Rev. Astr. Ap.*, **4**, 193.
———. 1968, in *Stars and Stellar Systems*, Vol. **7**, *Nebulae and Interstellar Matter*, ed. L. H. Aller and B. M. Middlehurst (Chicago: University of Chicago Press), p. 167.
Kuhi, L. V. 1964, *Ap. J.*, **140**, 1409.
Kwan, J., and Tademaru, E. 1988, *Ap. J. (Letters)*, **332**, L41.
Mundt, R., Brugel, E. W., and Bührke, T. 1987, *Ap. J.*, **319**, 275.
Murphy, D. C., Cohen, R., and May, J. 1986, *Astr. Ap.*, **167**, 234.
Norman, C. A., and Silk, J. 1980, *Ap. J.*, **238**, 158.
Osterbrock, D. E. 1989, *Astrophysics of Gaseous Nebulae and Active Galactic Nuclei* (Mill Valley, CA: University Science Books), p. 134.
Pudritz, R. E., and Norman, C. A. 1983, *Ap. J.*, **274**, 677.
Reipurth, B., Bally, J., Graham, J. A., Lane, A. P., and Zealey, W. J. 1986, *Astr. Ap.*, **164**, 51.
Schwartz, R. D. 1977, *Ap. J. Suppl.*, **35**, 161.
———. 1983, *Ann. Rev. Astr. Ap.*, **21**, 209.

Shu, F. H., Adams, F. C., and Lizano, S. 1987, *Ann. Rev. Astr. Ap.*, **25**, 23.
Snell, R. L. 1981, *Ap. J. Suppl.*, **45**, 121.
Snell, R. L., Loren, R. B., and Plambeck, R. L. 1980, *Ap. J. (Letters)*, **239**, L17.
Stone, R. P. S., and Baldwin, J. A. 1983, *M.N.R.A.S.*, **204**, 347.
Strom, S. E., Strom, K. M., and Edwards, S. 1988*a*, in *Galactic and Extragalactic Star Formation*, ed. Ralph Pudritz and Michel Fich (Dordrecht: Kluwer), p. 53.
Strom, K. M., Strom, S. E., Edwards, S., Cabrit, S., and Skrutskie, M. F. 1989, *A.J.*, **97**, 1451.
Strom, K. M., Strom, S. E., Kenyon, S. J., and Hartmann, L. 1988*b*, *A.J.*, **95**, 534.
Strom, K. M., Strom, S. E., Wolff, S. C., Morgan, J., and Wenz, M. 1986, *Ap. J. Suppl.*, **62**, 39.
Thé, P. S. 1962, *Contr. Bosscha Obs.*, No. 15.
Uchida, Y., and Shibata, K. 1985, *Pub. Astr. Soc. Japan*, **37**, 515.
Weber, E. J., and Davis, L. 1967, *Ap. J.*, **148**, 217.